Harriet C. Thoeny, MD[2]
Frederik De Keyzer, MSc
Feng Chen, MD
Yicheng Ni, MD, PhD
Willy Landuyt, PhD
Eric K. Verbeken, MD, PhD
Hilde Bosmans, MSc, PhD
Guy Marchal, MD, PhD
Robert Hermans, MD, PhD

Published online
10.1148/radiol.2343031721
Radiology 2005; 234:756–764

Abbreviations:
ADC = apparent diffusion coefficient
ROI = region of interest

[1] From the Departments of Radiology (H.C.T., F.D.K., F.C., Y.N., H.B., G.M., R.H.), Experimental Radiobiology/Laboratory of Experimental Oncology (W.L.), and Pathology (E.K.V.), University Hospitals Leuven, Herestraat 49, B-3000 Leuven, Belgium; and Department of Radiology, Zhong Da Hospital, Southeast University, Nanjing, China (F.C.). Received October 24, 2003; revision requested January 13, 2004; final revision received May 19; accepted June 17. H.C.T. supported by a grant from the Bernese Cancer League and by the Kurt and Senta Hermann Foundation. **Address correspondence to** Y.N. (e-mail: *yicheng.ni@med.kuleuven.ac.be*).

Authors stated no financial relationship to disclose.

Current address:
[2] Department of Diagnostic Radiology, University Hospital of Bern, Switzerland.

Author contributions:
Guarantors of integrity of entire study, G.M., R.H., W.L., H.C.T., Y.N.; study concepts, H.C.T., G.M., F.D.K., Y.N.; study design, H.C.T., F.D.K., G.M., W.L., H.B., Y.N.; literature research, H.C.T., W.L.; experimental studies, H.C.T., F.D.K., F.C., Y.N., W.L., H.B.; data acquisition, H.C.T., F.D.K., F.C., Y.N., W.L., H.B.; data analysis/interpretation, H.C.T., F.D.K., E.K.V., W.L., Y.N.; statistical analysis, F.D.K.; manuscript preparation, H.C.T., F.D.K., Y.N.; manuscript definition of intellectual content, H.C.T., F.D.K., R.H., G.M., W.L., Y.N.; manuscript editing, H.C.T., F.D.K., R.H., W.L., Y.N.; manuscript revision/review, H.C.T., F.D.K., R.H., Y.N.; manuscript final version approval, all authors

Diffusion-weighted MR Imaging in Monitoring the Effect of a Vascular Targeting Agent on Rhabdomyosarcoma in Rats[1]

PURPOSE: To evaluate diffusion-weighted magnetic resonance (MR) imaging for monitoring tumor response in rats after administration of combretastatin A4 phosphate.

MATERIALS AND METHODS: Study protocol was approved by local ethical committee for animal care and use. Rhabdomyosarcomas implanted subcutaneously in both flanks of 17 rats were evaluated with 1.5-T MR unit by using four-channel wrist coil. Transverse T2-weighted fast spin-echo sequences, T1-weighted spin-echo sequences before and after gadodiamide administration, and transverse echo-planar diffusion-weighted MR examinations were performed before, 1 and 6 hours, and 2 and 9 days after intraperitoneal injection of vascular targeting agent (combretastatin A4 phosphate, 25 mg/kg). Apparent diffusion coefficient (ADC) was automatically calculated from diffusion-weighted MR imaging findings. These findings were compared with histopathologic results at each time point. For statistical analysis, paired Student *t* tests with Bonferroni correction for multiple testing were used.

RESULTS: T1-weighted images before combretastatin administration showed enhancement of solid tumor tissue but not of central necrosis. At 1 and 6 hours after combretastatin injection, enhancement of solid tissue disappeared almost completely, with exception of small peripheral rim. At 2 and 9 days after combretastatin injection, enhancement progressively reappeared in tumor periphery. ADC, however, showed decrease early after combretastatin injection ($[1.26 \pm 0.16] \times 10^{-3}$ mm^2/sec before, $[1.18 \pm 0.17] \times 10^{-3}$ mm^2/sec 1 hour after [$P = .0005$] and $[1.08 \pm 0.14] \times 10^{-3}$ mm^2/sec 6 hours after [$P = .0007$] combretastatin A4 phosphate injection), histologically corresponding to vessel congestion and vascular shutdown in periphery but no necrosis. An increase of ADC ($[1.79 \pm 0.13] \times 10^{-3}$ mm^2/sec) ($P < .0001$) 2 days after combretastatin A4 phosphate injection was paralleled by progressive histologic necrosis. A significant ($P < .0001$) decrease in ADC 9 days after treatment ($[1.41 \pm 0.15] \times 10^{-3}$ mm^2/sec) corresponded to tumor regrowth.

CONCLUSION: In addition to basic relaxation-weighted MR imaging and post-gadolinium T1-weighted MR imaging to enable prompt detection of vascular shutdown, diffusion-weighted MR imaging was used to discriminate between nonperfused but viable and necrotic tumor tissues for early monitoring of therapeutic effects of vascular targeting agent.

Currently, there are two different therapeutic approaches used to induce tumor cell death at the vascular level; the first is to inhibit the formation of tumor blood vessels, and the

second is to selectively destroy them. Antiangiogenic agents prevent new vessel formation, whereas vascular targeting agents act selectively on preexisting blood vessels of solid tumors, which causes a rapid shutdown in the blood supply (1,2).

Combretastatin A4 phosphate is an antitubulin drug with inherent vascular targeting agent activity. To our knowledge, the precise mechanism of combretastatin induction of vascular shutdown is not fully understood (3,4); however, combretastatin is known to induce rapid changes in endothelial cell shape and to disrupt the endothelial cell layer and the underlying basement membranes. This leads to blood vessel congestion and loss of blood flow. Loss of oxygen and nutrient supply and impaired removal of metabolites induces cell death and consequent necrosis of the affected tumor tissue.

Combretastatin A4 phosphate has undergone phase 1 clinical trials (5–8). These studies showed tumor blood flow reduction in human tumors at well-tolerated doses, without persisting alteration of normal organs. Noninvasive monitoring of treatment response, including insight into typical intratumoral changes after the use of vascular targeting agents, is of major clinical importance.

Monitoring of clinical studies was performed mainly with dynamic contrast medium–enhanced magnetic resonance (MR) imaging or positron emission tomography (PET) (5,8). In addition to these modalities, experimental studies involved the use of scintigraphy, MR spectroscopy, radioactive tracer methods, and autoradiography to demonstrate early (eg, up to 24 hours) changes after combretastatin treatment (9–13).

Diffusion-weighted MR imaging is becoming more and more important in the assessment of tumors and evaluation of response during follow-up with various treatment modalities (eg, chemotherapy and radiation therapy) (14–18).

To our knowledge, there is only one study (9) in which treatment response with diffusion-weighted MR imaging after administration of combretastatin A4 phosphate was evaluated. In short-term follow-up (160 minutes after administration of combretastatin A4 phosphate), no substantial change could be observed (9). Thus, the purpose of our study was to evaluate diffusion-weighted MR imaging in monitoring response in rats after administration of the vascular targeting agent combretastatin A4 phosphate.

MATERIALS AND METHODS

Study Design

Our study protocol was approved by the local ethical committee for animal care and use.

Experiments were performed in 17 male adult WAG/Rij rats (Iffa Credo, Brussels, Belgium) that weighed 280–300 g each. Two rhabdomyosarcoma tumors (1-mm^3 pieces) were implanted subcutaneously (W.L.) in the flank region on opposite sides at the level of the kidneys. One tumor was implanted in each flank. The resultant 34 tumors had a baseline mean tumor volume of 2.34 $cm^3 \pm$ 0.62 (range, 1.93–3.78 cm^3) before treatment.

Five rats were examined during a follow-up period of 9 days after intraperitoneal administration of combretastatin A4 phosphate (Oxigene, Watertown, Mass) at a dose of 25 mg per kilogram of body weight and sacrificed thereafter. For histopathologic comparison at the intermediate time points of 1 hour, 6 hours, and 2 days after combretastatin A4 phosphate administration, three rats for each time point were sacrificed after examination with MR imaging. Three control rats underwent MR imaging before and 1 and 6 hours after intraperitoneal administration of a volume of saline identical to that of combretastatin A4 phosphate.

MR Imaging

The rats were examined with a 1.5-T whole-body MR system (Sonata; Siemens, Erlangen, Germany) with a maximum gradient capability of 40 mT/m. A four-channel phased-array wrist coil was used to obtain all MR images and allowed parallel imaging (generalized autocalibrating partially parallel acquisition, or GRAPPA, factor of two in all series). The rats were placed in the supine position in a plastic holder and connected with a mask to an anesthetic system to avoid movement. Rats were initially anesthetized with inhalation of 4% isoflurane; anesthesia was maintained with 2% isoflurane in a 20% oxygen and 80% room air mixture. The penile vein was cannulated for intravenous access.

A coronal T1-weighted spin-echo sequence was used as a localizer. Transverse T1-weighted spin-echo (repetition time msec/echo time msec, 553/15; matrix, 120 × 256) and T2-weighted turbo spin-echo sequences (5860/99; matrix, 160 × 256) were performed with a section thickness of 2 mm and an intersection gap of 0.2 mm. The field of view was 81.3 × 130.0 mm and covered both tumors entirely (20 sections).

The acquisition time was 1 minute 32 seconds for the T1-weighted sequence with two signals acquired and 1 minute 34 seconds for the T2-weighted sequence with three signals acquired.

Diffusion-weighted echo-planar imaging was performed with the following gradient factors: 0, 50, 100, 150, 200, 250, 300, 500, 750, and 1000 sec/mm^2. The following parameters were used for this sequence: 3300/124; matrix, 96 × 192; number of signals acquired, four; time of acquisition, 2 minutes 35 seconds. Apparent diffusion coefficient (ADC) maps were calculated automatically. ADC is measured in square millimeters per second.

After intravenous administration of 0.2 mL of gadodiamide (Omniscan; Amersham, Oslo, Norway) (0.5 mmol/L), a transverse T1-weighted spin-echo sequence was performed, with fat saturation identical to that obtained in the precontrast study.

All sequences were performed with the same geometry to maintain comparability between the different imaging sequences.

Image Analysis

The image analysis was performed offline at a Linux workstation by using dedicated software (Biomap; Novartis, Basel, Switzerland). In the transverse precontrast T1-weighted sequence, entire tumors were manually delineated on each section with consensus of two observers (H.C.T., 7 years of experience; F.D.K., 1 year of experience). Merging the delineations of each tumor yielded two three-dimensional regions of interest (ROIs), from which the system automatically calculated the average signal intensity of both tumors in each rat. The signal intensities of the conventional sequences were visually compared with muscle and graded as hypo-, iso-, or hyperintense. For the ADC maps, the same grading of the signal intensities was applied by comparing the center and the periphery of the tumor. The window and level settings of the display station were kept constant. This approach was chosen because ADC maps consist of absolute values.

Analysis of the diffusion-weighted MR images was performed. In the first step, ROIs of the T1-weighted images were copied to the ADC maps at each time point and manually adjusted in case of minor distortions that are sometimes visible on ADC maps and are caused by the echo-planar imaging sequence used. In

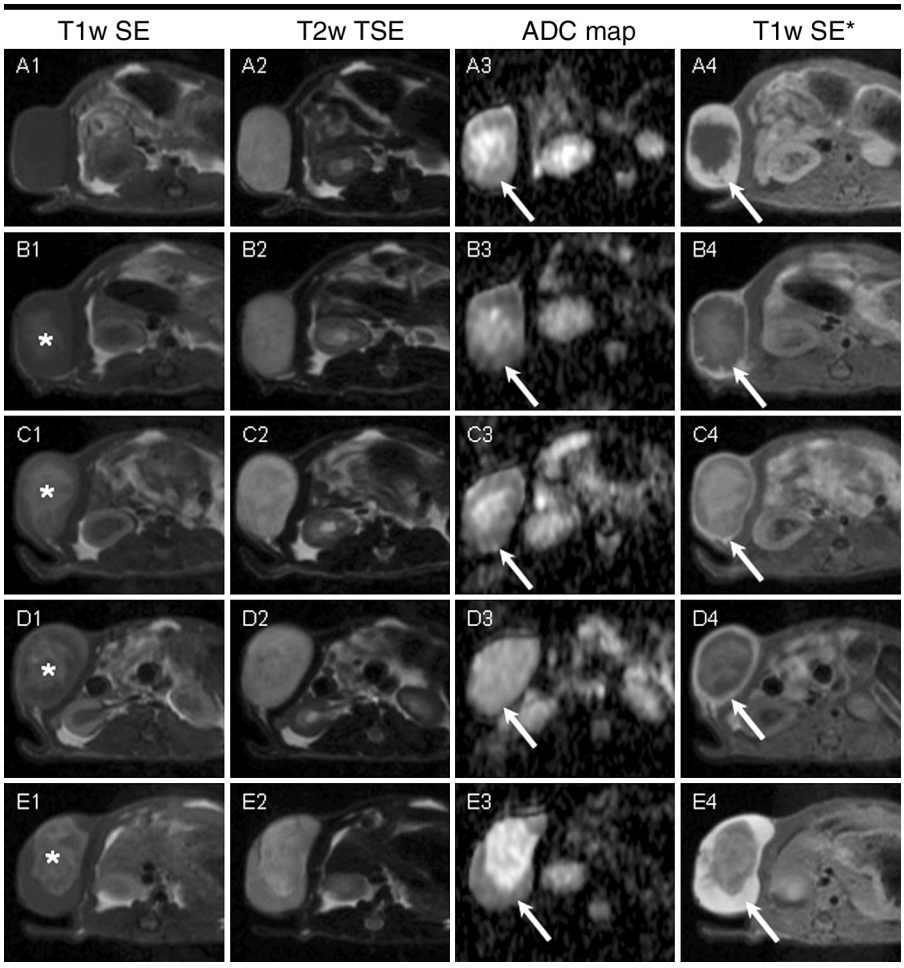

Figure 1. Overview of the effects of combretastatin A4 phosphate in the same animal before administration and 1 and 6 hours and 2 and 9 days after intraperitoneal administration. Before injection of combretastatin A4 phosphate, an enhancing rim of viable tumor tissue is seen on the transverse T1-weighted spin-echo contrast-enhanced MR image (553/15) (arrow in *A4*), which corresponds to the outer hypointense rim on the ADC map from the diffusion-weighted echo-planar imaging sequence (3300/124) (arrow in *A3*). The transverse T1-weighted contrast-enhanced images obtained 1 and 6 hours and 2 days after drug administration show a substantial decrease in the enhanced areas (arrow in *B4, C4,* and *D4*) when compared with the image obtained before combretastatin A4 phosphate injection (arrow in *A4*), which suggests extension of necrosis. The corresponding ADC maps, however, reveal necrosis only at 2-day follow-up (arrow in *D3*), with cells still intact at 1- and 6-hour follow-up (arrow in *B3* and *C3*), which is similar to the findings before drug administration (arrow in *A3*). The transverse T2-weighted images (5860/99) show a hyperintense signal of the entire tumor before combretastatin A4 phosphate administration, without substantial changes up to 2 days after combretastatin A4 phosphate administration (*A2, B2, C2,* and *D2*). Nine days after injection of combretastatin A4 phosphate, a regrowing rim of tumor tissue is apparent from the ADC map (arrow in *E3*), T2-weighted image (*E2*), and T1-weighted contrast-enhanced image (arrow in *E4*). The increase of signal intensity in the unenhanced T1-weighted images (*B1, C1, D1,* and *E1*) is caused by trapping of contrast medium in the central necrotic tumor area (*) from the previous contrast-enhanced images.

the second step, several circular ROIs were placed in the periphery (defined as the outer 5 mm) and in the center (more than 8 mm from the rim) of each tumor. Again, the respective ROIs were merged to obtain one center ROI and one peripheral ROI for each tumor. For comparison purposes, a circular ROI in the back muscles was drawn on a single section and copied from the T1-weighted images to the diffusion-weighted MR images. Afterward, the ROIs of the ADC maps were copied to the corresponding original diffusion-weighted images, from which the average intensities for each *b* value could be obtained.

In addition, ADCs of the tumors were calculated separately for low (0, 50, and 100 sec/mm^2) (ADC_{low}) and high (500, 750, and 1000 sec/mm^2) (ADC_{high}) *b* values to better differentiate the relative influence of the perfusion fraction and true diffusion.

ADCs were calculated by using a least squares solution of the following system of equations: $S(i) = S_0 \cdot \exp(-b_i \cdot ADC)$, where $S(i)$ is the signal intensity measured on the *i*'th *b* value image, and b_i is the corresponding *b* value. S_0 is a variable estimating the exact (without noise induced by the MR measurement) signal intensity for a *b* value of 0 sec/mm^2. To reduce influence of noise on the calculations, diffusion images with at least three different *b* values were used.

On the postcontrast T1-weighted images, the maximum diameter of the enhancing rim was measured in millimeters at each time point.

Histologic Analysis and Correlation with MR Imaging

After surgical excision of the tumors from the sacrificed rats at the previously mentioned time points, transsections were made in the transverse plane corresponding to the MR sections after fixation in 10% formaldehyde solution. Following paraffin embedding, 5-μm slices were stained with hematoxylin-eosin. All slices were examined by two pathologists in consensus (E.K.V. and Y.N., with 20 and 15 years of experience, respectively) by using magnification that ranged from ×12.5 to ×400. Tissue slices were microscopically assessed for the presence and extent of viable tumor cells and necrosis and for the status of intratumoral vasculature (eg, vessel patency, constriction, congestion, or dilatation). Thereafter, the histologic slices were compared with the corresponding spin-echo images and the ADC maps (H.C.T., W.L., E.K.V., and Y.N.). Comparison was based on viability of tumor cells versus necrosis, presence or absence of hemorrhage, and status of intratumoral vasculature at histologic analysis in relation to the enhanced versus unenhanced areas on the T1-weighted contrast material–enhanced MR images and the signal intensity on ADC maps.

Statistical Analysis

Statistical analysis was performed with Excel 9.0 (Microsoft, Seattle, Wash) and Analyse-It 1.68 (Analyse-it Software, Leeds, UK) software packages. Numeric data are reported as mean ± standard deviation.

Statistical analysis was performed by using a two-tailed paired Student *t* test with Bonferroni correction for multiple

TABLE 1
Average ADC of Entire Tumor

Time	ADC (mm^2/sec)*	ADC Low (mm^2/sec)†	ADC High (mm^2/sec)‡
Before administration of combretastatin A4 phosphate	$(1.26 \pm 0.16) \times 10^{-3}$	$(1.63 \pm 0.21) \times 10^{-3}$	$(1.17 \pm 0.17) \times 10^{-3}$
After administration of combretastatin A4 phosphate			
1 hour	$(1.18 \pm 0.17) \times 10^{-3}$	$(1.28 \pm 0.21) \times 10^{-3}$	$(1.10 \pm 0.17) \times 10^{-3}$
6 hours	$(1.08 \pm 0.14) \times 10^{-3}$	$(1.18 \pm 0.18) \times 10^{-3}$	$(1.03 \pm 0.14) \times 10^{-3}$
2 days	$(1.79 \pm 0.13) \times 10^{-3}$	$(2.01 \pm 0.19) \times 10^{-3}$	$(1.73 \pm 0.14) \times 10^{-3}$
9 days	$(1.41 \pm 0.15) \times 10^{-3}$	$(1.88 \pm 0.24) \times 10^{-3}$	$(1.22 \pm 0.17) \times 10^{-3}$

Note.—Data are mean ± standard deviation.
* Calculated from the entire *b* value setting.
† Calculated from lower *b* values (b = 0, 50, 100 sec/mm^2).
‡ Calculated from higher *b* values (b = 500, 750, 1000 sec/mm^2).

testing. A *P* value of less than .05 was considered to indicate a statistically significant difference. Retrospective power analysis was performed for all statistically significant results.

RESULTS

All tumors investigated exhibited the same behavior after combretastatin A4 phosphate injection; therefore, the results describe a generic tumor response. Morphologic evaluation of all tumors on the T1-weighted contrast-enhanced images yielded the same behavior at the respective time point after combretastatin A4 phosphate administration. This behavior was observed in all tumors during the entire observation time (28 tumors at 1 hour, 22 tumors at 6 hours, 16 tumors at 2 days, and 10 tumors at 9 days). No exception could be observed.

Before Combretastatin Injection

The T1-weighted images show homogeneous low signal intensity of the entire tumor; after gadodiamide administration, solid enhanced tissue with a central unenhanced area was visible (Fig 1, *A1, A4*). The corresponding T2-weighted images reveal slightly inhomogeneous high signal intensity of the tumors (Fig 1, *A2*).

The mean ADC of the entire tumor was $(1.26 \pm 0.16) \times 10^{-3}$ mm^2/sec (Table 1). The mean ADC calculated with low *b* values was significantly greater ($P < .0001$) than that calculated with high *b* values (Fig 2, Table 1). The ADC maps of the diffusion-weighted MR images at the same time point showed high signal intensity in the center (mean ADC, $[1.87 \pm 0.23] \times 10^{-3}$ mm^2/sec) (Fig 1, *A3*; Table 2) with a hypointense periphery (mean ADC, $[1.13 \pm 0.15] \times 10^{-3}$ mm^2/sec; $P < .0001$).

Histologic analysis in the control rats showed a central necrotic area that was completely surrounded by a thick peripheral layer of viable tumor cells with many mitoses. The periphery was sharply demarcated from the necrotic center. No edema or vascular congestion was present (Fig 3, *A3*). No changes were observed on the diffusion-weighted or conventional MR images after saline injection in the control rats.

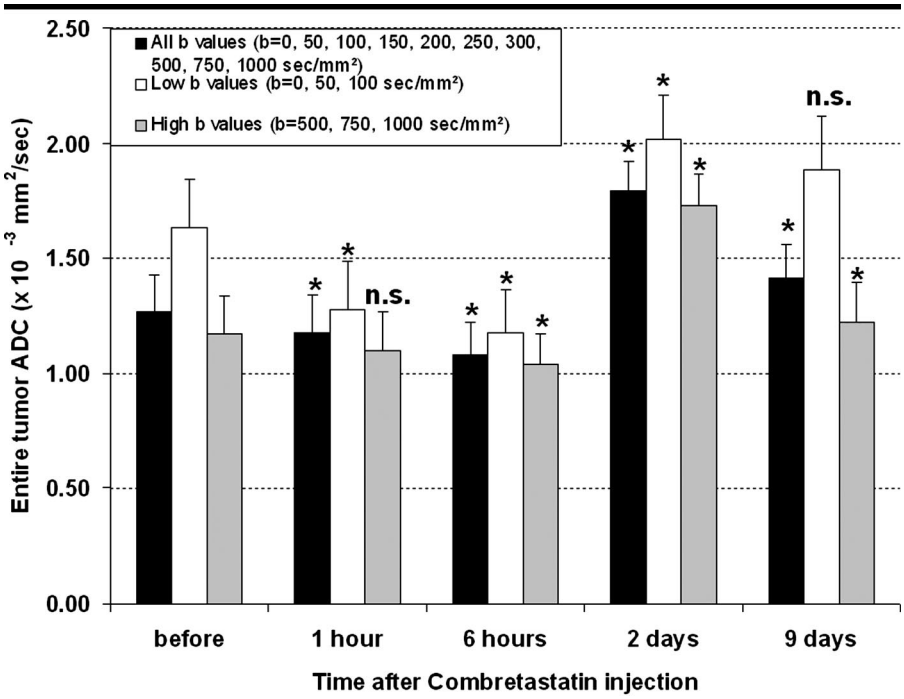

Figure 2. Averaged ADC of the entire tumor before and at different time points after intraperitoneal combretastatin A4 phosphate injection. The ADC_{low} decreases significantly ($P < .0001$) in the tumors 1 hour after intraperitoneal combretastatin A4 phosphate injection, which indicates reduction of blood perfusion in the early phase. From 1 to 6 hours after injection, the decrease is significant for ADC_{high} ($P = .02$) and ADC_{low} ($P = .02$), which suggests progressive decrease in blood flow and increased cell swelling. An increase at 2-day follow-up reflects progressive necrosis, whereas the significant decrease of ADC_{high} ($P < .0001$) from 2- to 9-day follow-up is consistent with tumor relapse. ∗ = Significant change compared to the previous time point. *n.s.* = No significant change compared to the previous time point.

Follow-up: 1 and 6 Hours after Combretastatin Injection

At 1 and 6 hours after administration of combretastatin A4 phosphate, a slightly increased signal intensity in the center of the tumor was observed on T1-weighted images, while a small peripheral enhancing rim was seen after gadodiamide administration (Fig 1, *B1* vs *B4*, *C1* vs *C4*). The central hyperintense area observed on images obtained at 6-hour follow-up was larger than that observed on images obtained at 1-hour follow-up (Fig 1, *B1, C1*). The T2-weighted images did not show any substantial visual changes up to 6 hours after combretastatin A4 phosphate injection. Also, the ADC maps at these time

TABLE 2
Average ADC of Center and Periphery of Tumor

Time	Center			Periphery		
	ADC (mm^2/sec)*	ADC Low (mm^2/sec)†	ADC High (mm^2/sec)‡	ADC (mm^2/sec)*	ADC Low (mm^2/sec)†	ADC High (mm^2/sec)‡
Before administration of combretastatin A4 phosphate	$(1.87 \pm 0.23) \times 10^{-3}$	$(1.99 \pm 0.28) \times 10^{-3}$	$(1.73 \pm 0.23) \times 10^{-3}$	$(1.13 \pm 0.15) \times 10^{-3}$	$(1.44 \pm 0.19) \times 10^{-3}$	$(1.08 \pm 0.17) \times 10^{-3}$
After administration of combretastatin A4 phosphate						
1 hour	$(1.81 \pm 0.22) \times 10^{-3}$	$(1.95 \pm 0.17) \times 10^{-3}$	$(1.71 \pm 0.21) \times 10^{-3}$	$(1.05 \pm 0.19) \times 10^{-3}$	$(1.14 \pm 0.25) \times 10^{-3}$	$(1.02 \pm 0.19) \times 10^{-3}$
6 hours	$(1.69 \pm 0.27) \times 10^{-3}$	$(1.88 \pm 0.35) \times 10^{-3}$	$(1.57 \pm 0.28) \times 10^{-3}$	$(0.98 \pm 0.18) \times 10^{-3}$	$(1.08 \pm 0.27) \times 10^{-3}$	$(0.96 \pm 0.16) \times 10^{-3}$
2 days	$(1.99 \pm 0.21) \times 10^{-3}$	$(2.08 \pm 0.18) \times 10^{-3}$	$(1.91 \pm 0.23) \times 10^{-3}$	$(1.84 \pm 0.30) \times 10^{-3}$	$(1.98 \pm 0.29) \times 10^{-3}$	$(1.73 \pm 0.28) \times 10^{-3}$
9 days	$(2.22 \pm 0.31) \times 10^{-3}$	$(2.41 \pm 0.28) \times 10^{-3}$	$(2.01 \pm 0.34) \times 10^{-3}$	$(1.03 \pm 0.18) \times 10^{-3}$	$(1.49 \pm 0.38) \times 10^{-3}$	$(0.98 \pm 0.15) \times 10^{-3}$

Note.—Data are mean ± standard deviation.
* Calculated from the entire *b* value setting.
† Calculated from lower *b* values (*b* = 0, 50, 100 sec/mm^2).
‡ Calculated from higher *b* values (*b* = 500, 750, 1000 sec/mm^2).

points were similar in appearance to those obtained before drug administration (Fig 1, *B2, B3, C2, C3*). However, the corresponding mean ADC of the entire tumor decreased progressively 1 hour ($P = .0005$) and 6 hours ($P = .0007$) after combretastatin A4 phosphate injection (Fig 2, Table 1), corresponding to decreases of the extracellular space. Histologic analysis showed that the decrease at 1 hour resulted from vascular collapse in the viable periphery with consequent crowding of endothelial cells (Fig 3, *B3*); the decrease at 6 hours resulted from pronounced edema throughout the periphery (Fig 3, *C3*). The respective ADC_{low} showed a significant decrease at 1 hour ($P < .0001$) and at 6 hours ($P = .02$). The ADC_{high} of the entire tumors remained mainly unchanged at 1 hour ($P = .08$) and showed only a slightly significant decrease at 6 hours ($P = .02$) (Table 1, Fig 2). The center did not reveal any significant change of the mean ADC, ADC_{high}, or ADC_{low} at 1 and 6 hours after combretastatin A4 phosphate injection. The mean ADC of the periphery also remained essentially unchanged (Fig 4, Table 2); however, the periphery decrease was significant for the ADC_{low} at 1 hour after injection ($P = .009$). At 6 hours, the ADC_{low} did not change significantly, and the ADC_{high} also remained relatively unchanged at both time points (Fig 4, Table 2).

The corresponding histologic specimens obtained 1 and 6 hours after intraperitoneal combretastatin A4 phosphate administration showed central necrosis at both time points. At 1-hour follow-up, constriction of the vessels in the periphery corresponded to the almost complete loss of enhancement on the T1-weighted images, with only a small remaining outer rim; the still hypointense rim on the ADC maps corresponded to still viable tumor cells (Fig 3, *B1, B2, B3*). At 6-hour follow-up, pronounced edema was observed. The blood vessels were dilated and congested; however, tumor cells remained viable (Fig 3, *C3*). Hemorrhage could not be observed with histologic analysis. Thus, the central hyperintensity on the T1-weighted precontrast images was attributed to trapping of gadolinium in the necrotic areas from the previous studies.

Follow-up: 2 Days after Combretastatin Injection

Two days after treatment, central signal intensity on the T1-weighted images decreased slightly (Fig 1, *D1*) in comparison to that of previous studies (Fig 1, *B1, C1*), with a small but slightly thickened peripheral enhancing rim remaining (Fig 1, *D4*; Fig 3). In most cases, the T2-weighted images were similar to those obtained in previous studies. The ADC maps showed inhomogeneous hyperintense tumors without differentiation of the center and periphery. The corresponding ADCs of the entire tumors increased significantly ($P < .0001$). The ADCs calculated from the low and high *b* values also increased significantly ($P < .0001$) (Fig 2, Table 1). The ADC of the center increased ($P = .02$); however, only the ADC_{high} increased significantly ($P = .002$), whereas the ADC_{low} remained mainly unchanged (Table 2, Fig 4). The ADC of the periphery increased significantly ($P < .0001$) for both ADC_{high} and ADC_{low}.

Histologic examination demonstrated enlargement of the necrotic area, and only a small rim of viable tissue at the outer periphery remained (Fig 3, *D3*).

Follow-up: 9 Days after Combretastatin Injection

Nine days after combretastatin A4 phosphate injection, the enhancing rim of the tumors thickened significantly ($P < .001$) (Fig 1, *E4*; Fig 3). The T2-weighted images showed a hyperintense center with a broad hypointense periphery. The mean ADC of the entire tumor at this time point decreased significantly compared with that measured 2 days after combretastatin A4 phosphate injection ($P < .0001$) (Table 1, Fig 2). The mean ADC of the center increased significantly ($P = .007$); however, the increase was only significant for ADC_{low} ($P = .0007$) and not for ADC_{high} (Fig 4, Table 2). In contrast, the ADC of the periphery decreased significantly ($P < .0001$) for ADC_{low} ($P = .009$) and ADC_{high} ($P < .0001$).

The corresponding histologic specimen revealed regrowth of solid tumor in the periphery in a centrifugal manner.

Follow-up of the solid enhancing rim is shown in the last column of Figure 1 (*A4, B4, C4, D4, E4*), and the corresponding measurements are shown in Figure 5.

The ADC of the muscle did not show any significant changes during the entire follow-up.

Retrospectively, the powers of all significant results were calculated. These ranged from .88 to 1, with the exception of one outlier, which only had a power of .67.

DISCUSSION

Vascular targeting agents such as combretastatin A4 phosphate are already in phase I clinical trials (5–8).

Intratumoral changes after this kind of treatment are important to recognize because in contrast to other anticancer therapies, such as use of cytotoxic agents and irradiation, a decrease in tumor volume is not an expected treatment response (19).

There are several requisites for an optimal imaging technique to monitor therapy response: The method should be noninvasive and quantitative, sample the entire tumor, be quick to perform, and allow repetition at frequent intervals.

Diffusion-weighted MR imaging has several potential advantages over other methods (eg, CT, PET, biopsy): It is noninvasive, without ionizing radiation exposure and the need for contrast medium administration, and it has a shorter examination time. The technique is easy to repeat, allowing close follow-up in cancer treatment. In addition, postprocessing is less time-consuming for diffusion-weighted MR imaging than for other methods (eg, dynamic contrast-enhanced MR imaging). In combination with conventional MR imaging, morphologic and physiologic changes can be assessed during the same examination.

Diffusion-weighted MR imaging allows monitoring of the entire tumor. This is very important because of the vast heterogeneity of most tumors. Tissue sampling is invasive and may not be representative of the entire tumor (20). Sampling also carries with it the inherent risks of infection, hemorrhage, and seeding along the needle track.

Diffusion-weighted MR imaging provides information about microscopic structures, such as cell density and integrity or necrosis (21). Thus, a viable tumor can be differentiated from a necrotic tumor with diffusion-weighted MR imaging (20) in contrast to conventional MR imaging.

Tissue with high cellular density shows low ADC resulting from impeded mobility of water protons by the higher amount of cell membranes (21,22), whereas necrotic tissue shows high ADC resulting from rapid diffusion of water protons as a consequence of lost membrane integrity (21). When analyzing the early effects of combretastatin A4 phosphate on tumors at 1 and 6 hours after drug administration with conventional contrast-enhanced images, the findings suggest necrosis of most parts of the previously viable tissue with the exception of a small solid rim in the periphery;

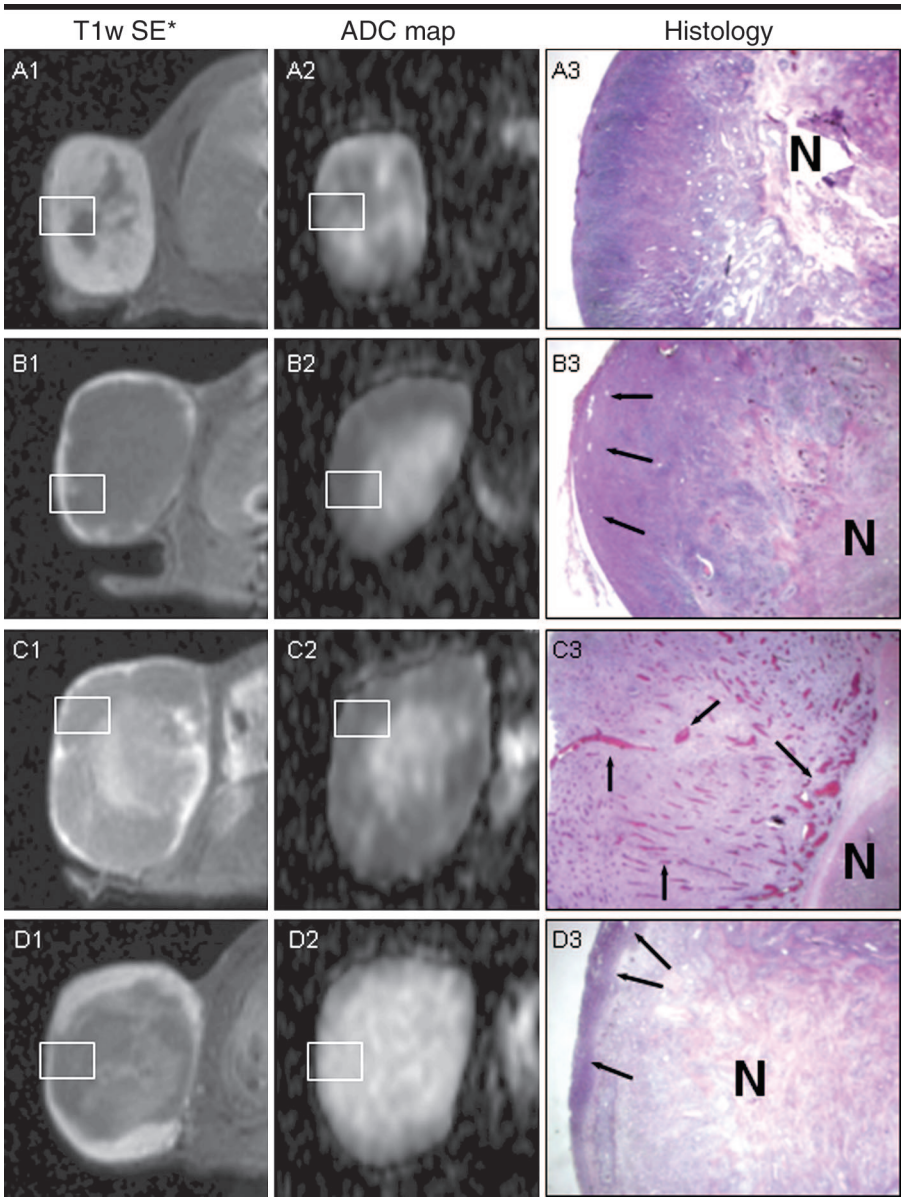

Figure 3. Comparison of transverse T1-weighted contrast-enhanced fat-saturated spin-echo MR image (553/15) *(A1–D1)*, ADC map *(A2–D2)* from the diffusion-weighted echo-planar images (3300/124), and histologic specimen (*A3–D3*) of the corresponding rat before *(A1–A3)*, 1 hour *(B1–B3)*, 6 hours *(C1–C3)*, and 2 days *(D1–D3)* after combretastatin A4 phosphate administration. The rectangular frames on the MR images indicate where the microscopic views were focused (hematoxylin-eosin stain; original magnification, ×12.5). Before combretastatin A4 phosphate injection, the enhancing tissue on the T1-weighted contrast-enhanced image *(A1)* corresponds to viable tumor tissue and patent blood vessels on the histologic slide *(A3)*. The central unenhanced area on the T1-weighted image and the hyperintensity on the ADC map *(A2)* correspond to the central necrosis *(A3)*. Early (1 and 6 hours) after combretastatin A4 phosphate injection, only a small enhancing peripheral rim with increase of the unenhanced areas is visible on the T1-weighted images *(B1* and *C1)*. On the ADC maps *(B2* and *C2)*, however, the peripheral rim is still broad, corresponding to viable tumor with vascular constriction except for peripheral vessels at 1-hour follow-up (arrows in *B3*) and multiple dilated and congested tumor vessels at 6-hour follow-up (arrows in *C3*). Two days after combretastatin A4 phosphate administration, the extent of unenhanced areas on the T1-weighted image *(D1)* and hyperintense area on the ADC map *(D2)* match with the necrosis seen on the histologic slide *(D3)*. In the periphery, only a small layer of viable tumor with patent blood vessels (arrows in *D3*) is visible. This explains the small enhancing rim on the T1-weighted image. *N* = necrosis.

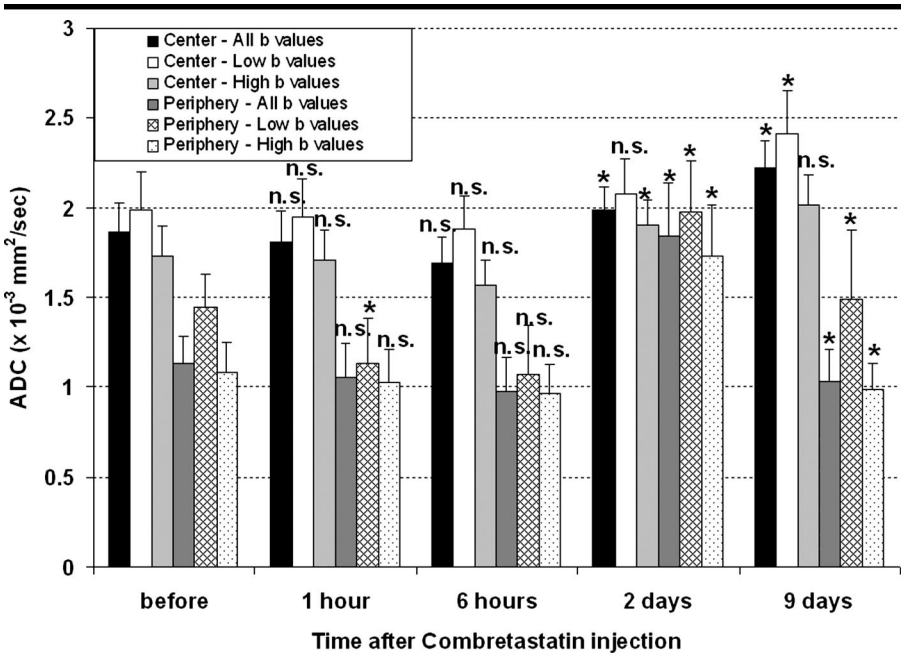

Figure 4. The ADCs of the center and the periphery are shown for all *b* values and for the low and the high *b* values separately. The ADC in the center does not change substantially in the early phase (up to 6 hours after combretastatin A4 phosphate injection). The ADC_{low} of the periphery, however, decreases substantially within 1 hour, which indicates a decrease of blood perfusion. An increase of the ADC_{low} and ADC_{high} in the periphery after 2 days reflects increased necrosis and an increase in perfused areas, which suggests early relapse in the periphery. The decrease of all ADCs from 2 to 9 days is consistent with tumor relapse in the periphery. ∗ = Significant change compared to the previous time point. *n.s.* = No significant change compared to the previous time point.

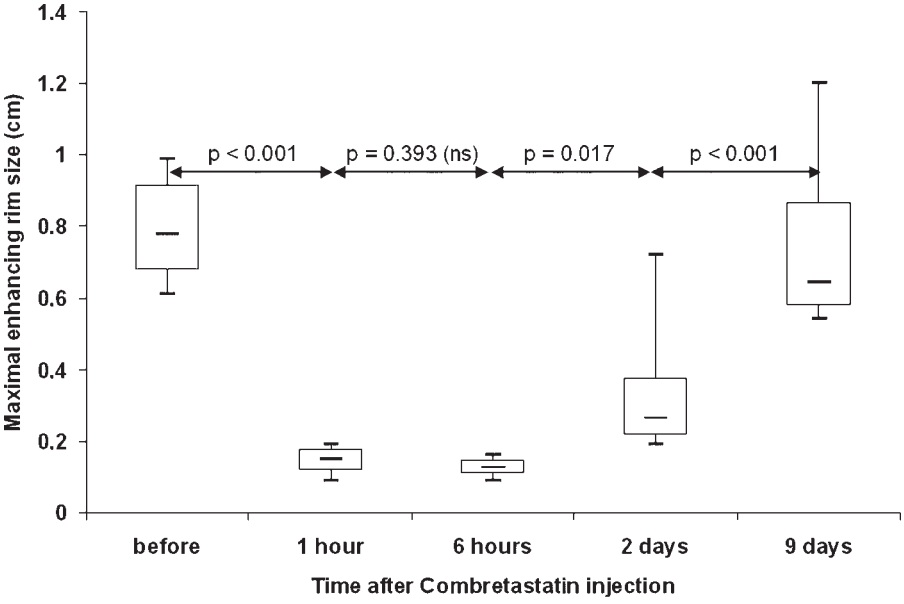

Figure 5. The maximal enhancing rim sizes, which were measured on T1-weighted MR images after administration of a large dose of gadodiamide, are given at different times before and after injection of combretastatin A4 phosphate. The rim size decreases significantly ($P < .001$) 1 hour after combretastatin A4 phosphate injection. There is still a decrease, although it is not statistically significant, during the next 5 hours. Significant regrowing of the rim is found 2 and 9 days after combretastatin A4 phosphate injection ($P = .017$ and $P < .001$, respectively).

however, diffusion-weighted MR imaging provides different information. Our results demonstrate that vascular shutdown appears early (1 and 6 hours) after combretastatin A4 phosphate injection, and this is only later followed by necrosis.

Thanks to the high sensitivity of diffusion-weighted MR imaging to molecular displacements in the orders of microns (three orders of magnitude less than the spatial resolution of a typical clinical MR examination), this method is very sensitive to biophysical changes related to tumors, even during their very early stages of development (23).

As a quantitative parameter of diffusion-weighted MR imaging, ADC reflects not only diffusion but also perfusion of microvessels (24). A large range of *b* values (b = 0, 50, 100, 150, 200, 250, 300, 500, 750, and 1000 sec/mm^2) was used to calculate two different ADCs. Those with low (0, 50, and 100 sec/mm^2) and those with high (500, 750, 1000 sec/mm^2) *b* values provide different information. Previous studies have shown that for low *b* values ($b < 100$ sec/mm^2), perfusion dominates diffusion by a factor of 10 (24,25). Thus, use of low and high *b* values in the same setting for calculation of ADC reflects contributions from both diffusion and perfusion effects, whereas a set of low *b* values is more weighted to the effects of perfusion. A set of high *b* values reduces the influence of perfusion and approximates true diffusion.

Early after treatment (1 and 6 hours), a significant decrease in the mean ADC of all tumors could be observed. This means diffusion is restricted, which can be attributed to early hemorrhage or ischemia—conditions that are not distinguishable on diffusion-weighted MR images alone (26). When analyzing the ADC of low and high *b* values separately, however, the decrease of the ADC of the low *b* values was more pronounced than the decrease of the high *b* values, which suggests a decrease mainly in perfusion due to vascular shutdown and probably consequent cell swelling. Furthermore, our results suggest that the most dramatic effect of combretastatin A4 phosphate on the tumor vasculature occurs within the first hour. Histologically, these findings corresponded to vessel constriction at 1 hour and vessel congestion at 6 hours. The remaining hypointense rim on the ADC map reflects a high cellular density, which represents the tumor cells still present in the histologic specimen. However, the contrast-enhanced T1-weighted images indicate almost complete disappearance of perfusion in the periphery, with only a small remaining rim suggesting peripheral extension of the necrotic area. Thus, the

conventional MR images provide an incomplete assessment of the changes in the tumor microenvironment.

A slightly progressive increase in central hyperintensity on the T1-weighted series from the images obtained at 1 and 6 hours could be seen. The corresponding histologic specimen did not show hemorrhage. The central hyperintensity seen on T1-weighted images was consistent with contrast medium from the previous studies trapped in the necrotic regions. This interpretation could be substantiated by a pilot study performed in tumor-bearing rats without treatment (data not shown).

Two days after combretastatin A4 phosphate injection, the conventional contrast-enhanced T1-weighted images showed the same extent of necrosis but with a slightly thickened peripheral rim when compared with the previous images. The corresponding ADC map and values showed substantial changes, which were suggestive of tumor cell damage and consequent necrosis.

The integrity of the cell membranes is compromised by the lack of nutrients with vascular shutdown, and the fractional volume of the interstitial space increases because of apoptotic body formation and cell loss. These changes increase the mobility of free water in the damaged tissue and are reflected by an increase in the ADC. Thus, successful therapy is expected to lead to a concomitant increase in ADC, a feature indeed observed in animal and human studies (27,28).

A rim of viable cells at the periphery is often observed after treatment with combretastatin A4 phosphate (29). There is a tendency of blood flow to recover more quickly in the peripheral tumor regions than in the central regions (13). The response of the peripheral vessels to combretastatin A4 phosphate treatment is reduced; the exact mechanism is unknown (12). This limits the effectiveness of combretastatin A4 phosphate administration and results in rapid regrowth of tumors after treatment (3).

The increase of ADC_{low} 2 days after treatment may reflect recovering blood flow in the tumor periphery. This rim can be targeted with adjuvant conventional cytotoxic approaches or radiation therapy (30–33).

The decrease of the entire tumor ADC from 2-day follow-up to 9-day follow-up after combretastatin A4 phosphate injection reflects tumor recurrence, a finding that can also be observed on the contrast-enhanced T1-weighted images with a large enhancing rim in the tumor periphery. This information cannot be obtained with conventional imaging methods without use of gadolinium.

Changes in ADC are more pronounced in the tumor periphery than in the center. Thus, the ADC of the entire tumor can be used for follow-up to provide information on the microenvironment of the entire tumor. The averaged values comprised both the peripheral and the central zone, and they are less discriminating over time; however, they still appropriately reflect changes in the tumor. Measuring ADC over the entire tumor has the further advantage of being easier to perform; also, selection bias of the investigator can be excluded when determining the different areas within the tumor.

Our findings of rapid reduction of tumor blood flow after combretastatin A4 phosphate injection corroborate findings of several studies in which other techniques were used (11,12,13,30,34); however, information pertaining to cellular integrity is only provided by diffusion-weighted MR imaging.

In contrast to most other experimental studies (11,12,13,34) in which high-field MR imaging is used, our experiments were performed with a clinical 1.5-T MR unit. As these machines allow parallel imaging, the resulting shorter examination time may be helpful in clinical trials.

A potential shortcoming of this study is the slight anatomic distortion present in the diffusion-weighted MR images and ADC maps when compared with the T1- and T2-weighted spin-echo images, which is caused by susceptibility effects in echo-planar imaging. This may reduce appreciation of intratumoral tissue heterogeneity with diffusion-weighted MR imaging. Also, as the number of time points investigated after injection of combretastatin A4 phosphate was limited, this study does not allow us to exactly determine the time point at which the tumor tissue converts from nonperfused but viable tissue to necrotic tissue.

Practical application: Diffusion-weighted MR imaging allows radiologists to detect and quantify intratumoral changes noninvasively after administration of a vascular targeting agent. In addition to basic relaxation-weighted MR imaging and postgadolinium T1-weighted MR imaging to promptly depict vascular shutdown, diffusion-weighted MR imaging was used to discriminate between nonperfused but viable tissue and necrotic tumor tissue for early monitoring of the therapeutic effects of a vascular targeting agent. Thus, it is a promising tool for monitoring the effects of such an agent.

Improved specificity of tumor tissue characterization would be a better guide to the care of patients with malignant tumors. It could potentially be used to predict treatment outcome and help radiologists make decisions about different treatment options.

References

1. Thorpe PE, Chaplin DJ, Blakey DC. The first international conference on vascular targeting: meeting overview. Cancer Res 2003; 63:1144–1147.
2. Denekamp J. Review article: angiogenesis, neovascular proliferation and vascular pathophysiology as targets for cancer therapy. Br J Radiol 1993; 66:181–196.
3. Tozer GM, Kanthou C, Parkins CS, Hill SA. The biology of the combretastatins as tumour vascular targeting agents. Int J Exp Pathol 2002; 83:21–38.
4. Kanthou C, Tozer GM. The tumor vascular targeting agent combretastatin A-4-phosphate induces reorganization of the actin cytoskeleton and early membrane blebbing in human endothelial cells. Blood 2002; 99:2060–2069.
5. Galbraith SM, Maxwell RJ, Lodge MA, et al. Combretastatin A4 phosphate has tumor antivascular activity in rat and man as demonstrated by dynamic magnetic resonance imaging. J Clin Oncol 2003; 21:2831–2842.
6. Rustin GJ, Galbraith SM, Anderson H, et al. Phase l clinical trial of weekly combretastatin A4 phosphate: clinical and pharmacokinetic results. J Clin Oncol 2003; 21:2815–2822.
7. Dowlati A, Robertson K, Cooney M, et al. A phase I pharmacokinetic and translational study of the novel vascular targeting agent combretastatin a-4 phosphate on a single-dose intravenous schedule in patients with advanced cancer. Cancer Res 2002; 62:3408–3416.
8. Anderson HL, Yap JT, Miller MP, Robbins A, Jones T, Price PM. Assessment of pharmacodynamic vascular response in a phase l trial of combretastatin A4 phosphate. J Clin Oncol 2003; 21:2823–2830.
9. Beauregard DA, Thelwall PE, Chaplin DJ, Hill SA, Adams GE, Brindle KM. Magnetic resonance imaging and spectroscopy of combretastatin A4 prodrug-induced disruption of tumour perfusion and energetic status. Br J Cancer 1998; 77:1761–1767.
10. Beauregard DA, Pedley RB, Hill SA, Brindle KM. Differential sensitivity of two adenocarcinoma xenografts to the anti-vascular drugs combretastatin A4 phosphate and 5,6-dimethylxanthenone-4-acetic acid, assessed using MRI and MRS. NMR Biomed 2002; 15:99–105.
11. Maxwell RJ, Wilson J, Prise VE, et al. Evaluation of the anti-vascular effects of combretastatin in rodent tumours by dynamic contrast enhanced MRI. NMR Biomed 2002; 15:89–98.
12. Tozer GM, Prise VE, Wilson J, et al. Combretastatin A-4 phosphate as a tumor vascular-targeting agent: early effects in tumors and normal tissues. Cancer Res 1999; 59:1626–1634.

13. Prise VE, Honess DJ, Stratford MR, Wilson J, Tozer GM. The vascular response of tumor and normal tissues in the rat to the vascular targeting agent, combretastatin A-4-phosphate, at clinically relevant doses. Int J Oncol 2002; 21:717–726.
14. Dzik-Jurasz A, Domenig C, George M, et al. Diffusion MRI for prediction of response of rectal cancer to chemoradiation. Lancet 2002; 360:307–308.
15. Yamada I, Aung W, Himeno Y, Nakagawa T, Shibuya H. Diffusion coefficients in abdominal organs and hepatic lesions: evaluation with intravoxel incoherent motion echo-planar MR imaging. Radiology 1999; 210:617–623.
16. Taouli B, Vilgrain V, Dumont E, Daire JL, Fan B, Menu Y. Evaluation of liver diffusion isotropy and characterization of focal hepatic lesions with two single-shot echo-planar MR imaging sequences: prospective study in 66 patients. Radiology 2003; 226:71–78.
17. Jennings D, Hatton BN, Guo J, et al. Early response of prostate carcinoma xenografts to docetaxel chemotherapy monitored with diffusion MRI. Neoplasia 2002; 4:255–262.
18. DeVries AF, Kremser C, Hein PA, et al. Tumor microcirculation and diffusion predict therapy outcome for primary rectal carcinoma. Int J Radiat Oncol Biol Phys 2003; 56:958–965.
19. Hori K, Saito S, Sato Y, et al. Differential relationship between changes in tumour size and microcirculatory functions induced by therapy with an antivascular drug and with cytotoxic drugs: implications for the evaluation of therapeutic efficacy of AC7700 (AVE8062). Eur J Cancer 2003; 39:1957–1966.
20. Lang P, Wendland MF, Saeed M, et al. Osteogenic sarcoma: noninvasive in vivo assessment of tumor necrosis with diffusion-weighted MR imaging. Radiology 1998; 206:227–235.
21. Lyng H, Haraldseth O, Rofstad EK. Measurement of cell density and necrotic fraction in human melanoma xenografts by diffusion weighted magnetic resonance imaging. Magn Reson Med 2000; 43:828–836.
22. Sugahara T, Korogi Y, Kochi M, et al. Usefulness of diffusion-weighted MRI with echo-planar technique in the evaluation of cellularity in gliomas. J Magn Reson Imaging 1999; 9:53–60.
23. Wheeler-Kingshott CA, Thomas DL, Lythgoe MF, Guilfoyle D, Williams SR, Doran SJ. Burst excitation for quantitative diffusion imaging with multiple b-values. Magn Reson Med 2000; 44:737–745.
24. Le Bihan D, Breton E, Lallemand D, Aubin ML, Vignaud J, Laval-Jeantet M. Separation of diffusion and perfusion in intravoxel incoherent motion MR imaging. Radiology 1988; 168:497–505.
25. Morvan D. In vivo measurement of diffusion and pseudo-diffusion in skeletal muscle at rest and after exercise. Magn Reson Imaging 1995; 13:193–199.
26. Atlas SW, DuBois P, Singer MB, Lu D. Diffusion measurements in intracranial hematomas: implications for MR imaging of acute stroke. AJNR Am J Neuroradiol 2000; 21:1190–1194.
27. Galons JP, Altbach MI, Paine-Murrieta GD, Taylor CW, Gillies RJ. Early increases in breast tumor xenograft water mobility in response to paclitaxel therapy detected by non-invasive diffusion magnetic resonance imaging. Neoplasia 1999; 1:113–117.
28. Chenevert TL, Stegman LD, Taylor JM, et al. Diffusion magnetic resonance imaging: an early surrogate marker of therapeutic efficacy in brain tumors. J Natl Cancer Inst 2000; 92:2029–2035.
29. Dark GG, Hill SA, Prise VE, Tozer GM, Pettit GR, Chaplin DJ. Combretastatin A-4, an agent that displays potent and selective toxicity toward tumor vasculature. Cancer Res 1997; 57:1829–1834.
30. Landuyt W, Ahmed B, Nuyts S, et al. In vivo antitumor effect of vascular targeting combined with either ionizing radiation or anti-angiogenesis treatment. Int J Radiat Oncol Biol Phys 2001; 49:443–450.
31. Siemann DW, Mercer E, Lepler S, Rojiani AM. Vascular targeting agents enhance chemotherapeutic agent activities in solid tumor therapy. Int J Cancer 2002; 99:1–6.
32. Wachsberger P, Burd R, Dicker AP. Tumor response to ionizing radiation combined with antiangiogenesis or vascular targeting agents: exploring mechanisms of interaction. Clin Cancer Res 2003; 9:1957–1971.
33. Ma BB, Bristow RG, Kim J, Siu LL. Combined-modality treatment of solid tumors using radiotherapy and molecular targeted agents. J Clin Oncol 2003; 21:2760–2776.
34. Beauregard DA, Hill SA, Chaplin DJ, Brindle KM. The susceptibility of tumors to the antivascular drug combretastatin A4 phosphate correlates with vascular permeability. Cancer Res 2001; 61:6811–6815.